Asynchronous and slow-wave oscillatory states in connectome-based models of mouse, monkey and human cerebral cortex

Jennifer S. Goldman[a,b], Maria Sacha[a,b], Lionel Kusch[c] and Alain Destexhe[a,*]

[a]Paris-Saclay University, CNRS, Paris-Saclay Institute of Neuroscience (NeuroPSI), 91400 Saclay, France
[b]co-first authors
[c]Institut de Neurosciences des Systèmes, Aix-Marseille University, INSERM, Marseille, France

ARTICLE INFO

Keywords:
Cerebral cortex
Asynchronous states
Slow oscillations
Sleep
Computational models
Mean-field models

ABSTRACT

Thanks to the availability of connectome data that map connectivity between multiple brain areas, it is now possible to build models of whole brain activity. At the same time, advances in mean-field techniques have led to biologically based population models that integrate biophysical features such as membrane conductances or synaptic conductances. In this paper, we show that this approach can lead to brain-wide models of mouse, macaque, and human. We illustrate this approach by showing the transition from wakefulness to sleep simulated with multi-scale models in the three species. We compare the level of synchrony between the three species and found that the mouse brain displays a higher overall synchrony of slow-waves compared to monkey and human brains. We also make the program code publicly available, which provides a set of open-source tools for simulating large-scale activity in the cerebral cortex of mouse, monkey, and human.

1. Introduction

Brain activity can display widely different states of activity, ranging from the two extremes of asynchronous activity, typical of the aroused brain, and slow and synchronized oscillatory states, reminiscent of slow-wave sleep or anesthesia (Steriade, 2003; Niedermeyer and Lopes da Silva, 2005). To model such "macroscopic" states of brain activity, one should ideally take into account "microscopic" features that are key to the genesis of brain states. Therefore, models that can account for biophysical features of brain states must be multi-scale. At the microscopic scale, the genesis of neural activity depends on membrane conductances, such as those responsible for spike-frequency adaptation, which regulate transitions between activity states in cortical slices (Compte et al., 2003). The macroscopic features of neural activity between brain states may also crucially depend on recurrent connectivity between excitatory and inhibitory neuron types in cerebral cortex. Here, computational models have been successful to simulate such activity states, either the asynchronous-irregular state (Van Vreeswijk and Sompolinsky, 1996; Brunel, 2000; Compte et al., 2003; Zerlaut et al., 2018), or the slow-wave state with "Up" and "Down" state dynamics (Bazhenov et al., 2002; Compte et al., 2003; di Volo et al., 2019). Few models could simulate both states, however, because their transition depends on the presence of spike-frequency adaptation conductances. These transitions can be modeled either by Hodgkin-Huxley type models (Compte et al., 2003) or by integrate-and-fire type models that include spike-frequency adaptation such as the Adaptive Exponential (AdEx) model (di Volo et al., 2019).

Although the genesis of asynchronous and slow oscillatory states can be well modeled at the local network scale, as typically based on *in vitro* activity (Sanchez-Vives and McCormick, 2000), it is less clear how such activity is organized at larger scales. Here, the activities generated at local scale in each brain area interact through the long-range inter-areal connectivity. The precise pattern of inter-areal connectivity is provided by the connectome, which has been published open-access for a number of species such as mouse (Oh et al., 2014), macaque monkey (Kötter, 2004) and human (Van Essen et al., 2012). So the information is available to construct large-scale models that will include all brain areas and their connectivity. However, simulating such models at the cellular scale represents a huge investment of computational resources, and is out of reach for most researchers having no access to such resources.

An alternative approach is to simulate brain activity using population models, which are much less demanding on computational resources. However, such models need to have enough biological realism to include the relevant biophysical mechanisms necessary to generate brain states, as described above, such as membrane conductances, synaptic receptor types, etc. We will use here an approach that was provided in a recent series of papers (Zerlaut et al., 2018; di Volo et al., 2019; Goldman et al., 2020, 2022). A mean-field model was first derived for AdEx spiking networks (Zerlaut et al., 2018; di Volo et al., 2019) and successfully generated both asynchronous and synchronized slow-wave dynamics, and their transition by controlling spike-frequency adaptation, as in the experiments. This AdEx mean-field model is much faster to simulate than the spiking networks. Next, such mean-field models were integrated into large-scale models of the human brain (Goldman et al., 2020, 2022) and could successfully simulate asynchronous states, similar to wakefulness, and slow-wave oscillatory states, similar to slow-wave sleep, as well as their responsiveness to external stimuli (for a similar approach using current-based models, see Cakan et al. (2022)).

*Corresponding author
alain.destexhe@cnrs.fr (A. Destexhe)
ORCID(s): 0000-0001-7405-0455 (A. Destexhe)

In the present paper, we extend this approach to two species, mouse and macaque monkey. We show the integration of the AdEx mean-field models into large-scale models of the entire cerebral cortex, comparing three species, mouse, monkey and human. In particular, we will illustrate the simulated brain dynamics for asynchronous and slow-wave activity, across the whole cerebral cortex.

2. Methods

We used three types of models, a network of spiking neurons, a mean-field model of this network, and a network of mean-field models implemented in The Virtual Brain (TVB). We describe here these models successively.

2.1. Spiking network model

We considered networks of integrate-and-fire neuron models displaying spike-frequency adaptation, based on two previous papers (Destexhe, 2009; Zerlaut et al., 2018). We used the Adaptive Exponential (AdEx) integrate-and-fire model (Brette and Gerstner, 2005). We considered a population of $N = 10^4$ neurons randomly connected with a connection probability of $p = 5\%$. We considered excitatory and inhibitory neurons, with 20% inhibitory neurons. The AdEx model allows us to define two cell types, "regular-spiking" (RS) excitatory cells, displaying spike-frequency adaptation, and "fast spiking" (FS) inhibitory cells, with no adaptation. The dynamics of these neurons is given by the following equations:

$$\begin{aligned} c_m \frac{dv_k}{dt} &= g_L(E_L - v_k) + \Delta e^{\frac{v_k - v_{thr}}{\Delta}} - w_k + I_{syn} \\ \tau_w \frac{dw_k}{dt} &= -w_k + b \sum_{t_{sp}(k)} \delta(t - t_{sp}(k)) \\ &\quad + a(v_k - E_L), \end{aligned} \tag{1}$$

where $c_m = 200$ pF is the membrane capacitance, v_k is the voltage of neuron k and, whenever $v_k > v_{thr} = -50$ mV at time $t_{sp}(k)$, v_k is reset to the resting voltage $v_{rest} = -65$ mV and fixed to that value for a refractory period $T_{refr} = 5$ ms. The leak term g_L had a fixed conductance of $g_L = 10$ nS and the leakage reversal E_L was of -65 mV. The exponential term had a different strength for RS and FS cells, i.e. $\Delta = 2$mV ($\Delta = 0.5$mV) for excitatory (inhibitory) cells. Inhibitory neurons were modeled as fast spiking FS neurons without adaptation ($a = b = 0$ for all inhibitory neurons) whereas excitatory regular spiking RS neurons had a lower level of excitability due to the presence of adaptation (while b varied in our simulations we fixed $a = 4$ nS and $\tau_w = 500$ ms unless otherwise specified). The synaptic current I_{syn} received by neuron i is the result of the spiking activity of all neurons $j \in \text{pre}(i)$ pre-synaptic to neuron i. This current can be decomposed in the synaptic conductances evoked by excitatory E and inhibitory I pre-synaptic spikes

$$I_{syn} = G^e_{syn}(E_e - v_k) + G^i_{syn}(E_i - v_k) \,,$$

where $E_e = 0$mV ($E_i = -80$mV) is the excitatory (inhibitory) reversal potential. Excitatory synaptic conductances were modeled by a decaying exponential function that sharply increases by a fixed amount Q_E at each pre-synaptic spike, i.e.:

$$G^e_{syn}(t) = Q_e \sum_{exc.pre} \Theta(t - t^e_{sp}(k))\, e^{-(t - t^e_{sp}(k))/\tau_e} \,,$$

where Θ is the Heaviside function, $\tau_e = \tau_i = 5$ms is the characteristic decay time of excitatory and inhibitory synaptic conductances, and $Q_e = 1$ nS ($Q_i = 5$ nS) the excitatory (inhibitory) quantal conductance. Inhibitory synaptic conductances are modeled using the same equation with $e \to i$. This network displays two different states according to the level of adaptation, $b = 5$ pA for asynchronous-irregular states, and $b = 60$ pA for Up-Down states (Fig. 1A; see Zerlaut et al. (2018) for details).

2.2. Mean-field models

We considered a population model of a network of AdEx neurons, using a Master Equation formalism originally developed for balanced networks of integrate-and-fire neurons (El Boustani and Destexhe, 2009). This model was adapted to AdEx networks of RS and FS neurons (Zerlaut et al., 2018), and later modified to include adaptation (di Volo et al., 2019). The latter version is used here, which corresponds to the following equations:

$$\begin{aligned} T\frac{\partial \nu_\mu}{\partial t} &= (F_\mu - \nu_\mu) + \frac{1}{2} c_{\lambda\eta} \frac{\partial^2 F_\mu}{\partial \nu_\lambda \partial \nu_\eta} \\ T\frac{\partial c_{\lambda\eta}}{\partial t} &= \delta_{\lambda\eta} \frac{F_\lambda(1/T - F_\eta)}{N_\lambda} + (F_\lambda - \nu_\lambda)(F_\eta - \nu_\eta) \\ &\quad + \frac{\partial F_\lambda}{\partial \nu_\mu} c_{\eta\mu} + \frac{\partial F_\eta}{\partial \nu_\mu} c_{\lambda\mu} - 2c_{\lambda\eta} \\ \tau_w \frac{\partial W}{\partial t} &= -W + b\tau_w \nu_e + a(\mu_V(\nu_e, \nu_i, W) - E_L) \,, \end{aligned} \tag{2}$$

where $\mu = \{e, i\}$ is the population index (excitatory or inhibitory), ν_μ the population firing rate and $c_{\lambda\eta}$ the covariance between populations λ and η. W is a population adaptation variable (di Volo et al., 2019). $\delta_{\lambda\eta}$=1 if $\lambda = \eta$ and zero otherwise. The function $F_{\mu=\{e,i\}} = F_{\mu=\{e,i\}}(\nu_e, \nu_i, W)$ is the transfer function which describes the firing rate of population μ as a function of excitatory and inhibitory inputs (with rates ν_e and ν_i) and adaptation level W. These functions were estimated previously for RS and FS cells and in the presence of adaptation (di Volo et al., 2019).

At the first order, i.e. neglecting the dynamics of the covariance terms $c_{\lambda\eta}$, this model can be written simply as:

$$T\frac{d\nu_\mu}{dt} = (F_\mu - \nu_\mu) \,, \tag{3}$$

together with Eq. 3. This system is equivalent to the well-known Wilson-Cowan model (Wilson and Cowan, 1972), with the specificity that the functions F need to be obtained according to the specific single neuron model under consideration. These functions were obtained previously for AdEx models of RS and FS cells (Zerlaut et al., 2018; di Volo et al., 2019) and the same are used here.

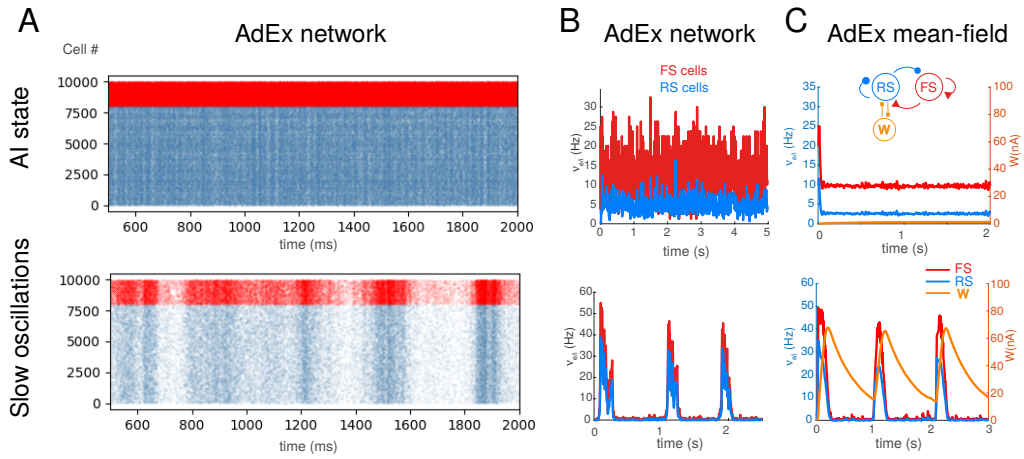

Figure 1: Asynchronous-irregular and slow oscillatory states in AdEx networks and mean-field models. A. Raster plots of excitatory RS (blue) and inhibitory FS (red) AdEx neurons in a network during asynchronous-irregular (AI) state (top), and slow oscillations with Up and Down states (bottom). The two states differed from the values of adaptation parameter b (b=1 pA for AI state, and 20 pA for slow oscillations shown here). B. Corresponding mean firing rates of the two populations. C. Mean-field model of AdEx networks with adaptation (scheme in inset). The mean-field reproduces the two states and the corresponding firing rate variations. Modified from di Volo et al. (2019); Capone et al. (2019); Goldman et al. (2020).

For a cortical volume modeled as a two populations of excitatory and inhibitory neurons, the equations (at first order) can be written as:

$$\begin{aligned} T\frac{d\nu_e}{dt} &= \mathcal{F}_e(\nu_e + \nu_{aff} + \nu_{drive}, \nu_i) - \nu_e \\ T\frac{d\nu_i}{dt} &= \mathcal{F}_i(\nu_e + \nu_{aff}, \nu_i) - \nu_i \\ \tau_w\frac{dW}{dt} &= -W + b\tau_w\nu_e + a(\mu_V(\nu_e, \nu_i, W) - E_L)\,, \end{aligned} \tag{4}$$

where ν_{aff} is the afferent thalamic input to the population of excitatory and inhibitory neurons and ν_{drive} is an external noisy drive. The function μ_V is the average membrane potential of the population and is given by

$$\mu_V = \frac{\mu_{Ge}E_e + \mu_{Gi}E + i + g_L E_L - W}{\mu_{Ge} + \mu_{Gi} + g_L}\,,$$

where the mean excitatory conductance is $\mu_{Ge} = \nu_e K_e \tau_e Q_e$ and similarly for inhibition.

This system describes the population dynamics of a single isolated cortical column, and was shown to closely match the dynamics of the spiking network (Fig. 1; di Volo et al. (2019)).

2.3. Networks of mean-field models

Extending our previous work at the mesoscale (di Volo et al., 2019; Chemla et al., 2019) to model large brain regions, we define networks of mean-field models, representing interconnected cortical columns (each described by a mean-field model). For simplicity, we considered only excitatory interactions between cortical columns, while inhibitory connections remain local to each column. The equations of such a network, expanding the two-population mean-field (Eq. 4), are given by:

$$\begin{aligned} T\frac{d\nu_e(k)}{dt} &= \mathcal{F}_e\left[\nu_e^{input}(k) + \nu_{aff}(k), \nu_i(k)\right] - \nu_e(k) \\ T\frac{d\nu_i(k)}{dt} &= \mathcal{F}_i\left[\nu_e^{input}(k) + \nu_{aff}(k), \nu_i(k)\right] - \nu_i(k) \\ \tau_w\frac{dW(k)}{dt} &= -W(k) + b\tau_w\nu_e(k) \\ &\quad + a(\mu_V(\nu_e(k), \nu_i(k), W(k)) - E_L)\,, \end{aligned} \tag{5}$$

where $\nu_e(k)$ and $\nu_i(k)$ are the excitatory and inhibitory population firing rates at site k, respectively, $W(k)$ the level of adapation of the population, and $\nu_e^{input}(k)$ is the excitatory synaptic input. The latter is given by:

$$\nu_e^{input}(k) = \nu_{drive}(k) + \sum_j C_{jk}\,\nu_e(j, t - \|j-k\|/v_c) \tag{6}$$

where the sum runs over all nodes j sending excitatory connections to node k, and C_{jk} is the strength of the connection from j to k (and is equal to 1 for $j = k$). Note that $\nu_e(j, t - \|j-k\|/v_c)$ is the activity of the excitatory population at node k at time $t - \|j-k\|/v_c$ to account for the delay of axonal propagation. Here, $\|j-k\|$ is the distance between nodes j and k and v_c is the axonal propagation speed.

2.4. Integration in The Virtual Brain

The integration of networks of mean-field models was done for each species using The Virtual Brain (TVB) simulator (https://www.thevirtualbrain.org/tvb). For the mouse brain, we used "The Virtual Mouse Brain" (Melozzi et al., 2017), the monkey brain model was given by the macaque TVB (Shen et al., 2019), and the TVB model of the human brain was from Jirsa et al. (2017). These publications should be consulted for details about the connectivity used. The particular implementation of the human TVB was that given in Goldman et al. (2022), where more details can be obtained.

2.5. Analysis

To quantify the amount of synchrony in the TVB model, we computed the Phase-Lag Index (PLI) for each pair of

nodes, averaged over the simulation time. The Hilbert transform is first computed to extract the phase $\psi(t)$ of the time series. From there, the PLI is given by

$$\text{PLI} \equiv |< sign(\psi_i(t) - \psi_j(t)) >|, \tag{7}$$

where $< \cdot >$ denotes averaging over time, for nodes i and j (Silva Pereira et al., 2017). Note that the PLI takes values between 0 (random phase relations or perfect synchrony) and 1 (perfect phase locking). In this work we report the mean PLI over all time epochs for excitatory and inhibitory firing rates of each region pair for each adaptation value.

2.6. Code availability

The code source of all simulations shown in this article is available online. A repository is available in *Zenodo* (Goldman et al., 2023), and the code can be run online using the simulation capabilities offered by the Human Brain Project's EBRAINS neuroscience research infrastructure (`https://ebrains.eu` and `https://ebrains.eu/service/the-virtual-brain`).

3. Results

We start by showing the behavior of the mean-field model, then we show its integration in brain-wide models of mouse, monkey and human cerebral cortex.

Figure 1 shows the spiking network model of AdEx neurons, comprising RS (blue) and FS (red) cells, as detailed in previous studies (Zerlaut et al., 2018; di Volo et al., 2019). This network can generate asynchronous irregular (AI) activity states (Fig. 1A, top), as well as slow synchronized activity under the form of Up and Down states (Fig. 1A, bottom). The transition from these two states is obtained by strengthening or weakening of the spike-frequency adaptation in RS cells (parameter b in the model). The mean rates of activity of these two states are shown in Fig. 1B, respectively. The mean-field model of this AdEx network was derived in two previous publications (Zerlaut et al., 2018; di Volo et al., 2019) and is shown for these two states in Fig. 1C.

As shown previously (Goldman et al., 2020, 2022), the AdEx mean-field model was implemented in The Virtual Brain (TVB) platform. This platform consists of a python-based simulation environment (Jirsa et al., 2017) which allows the user to create a network of mean-field models (or more generally neural mass models), constrained by connectivity data extracted from a given connectome. The TVB environment can also generate a number of neural signals and be linked to neuro-imaging (Ritter et al., 2013). Integrating the AdEx mean-field in TVB, leading to the "TVB-AdEx" model (Goldman et al., 2020), has a double advantage. First, the mean-field model is biologically informed, so it has physically-interpretable parameters (such as conductances, synaptic receptor kinetics, etc) that can be changed and directly compared to experiments. Second, the AdEx mean-field can generate states of activity which can be asynchronous or synchronized (see Fig. 1), which is not the case with other neural mass models.

The behavior of the TVB-AdEx model is illustrated in Fig. 2. In all three species, the asynchronous activity of the mean-field model leads to a global dynamics which is also asynchronous (Fig. 2, middle panels). While there were some variations of the absolute amplitudes of the firing rates, the three models displayed consistent asynchronous dynamics. For higher levels of adaptation, the three models displayed slow-wave activity, as in the mean-field model. However, in this case the individual nodes synchronized their slow oscillation, which generated a globally synchronized slow-wave activity across large brain regions. In the case of the human brain, a grid scan of parameters showed that the level of synchrony depends on the parameters, and in particular on the strength of the long-range connectivity (Goldman et al., 2022). Similar behavior was observed in the three models illustrated here (not shown).

The comparison of the two states across the models of the three species is further shown in Fig. 3. The transition from asynchronous to slow-wave dynamics occurs at about the same value of adaptation parameter b (Fig. 3A). Interestingly, the duration of the down states is predicted to be similar between species. One can also see that the down-state duration increases with b, and thus the slow-wave frequency will also decrease proportionally to the level of adaptation. The level of synchrony of the activities is shown in Figs. 3B-C, as measured by the phase-lag index (PLI), for excitatory and inhibitory population activities, respectively. The synchrony increases for excitatory cells as a function of the adaptation parameter b, but only for excitatory populations. However, the tendency to increase synchrony with b is unclear with inhibitory populations (Fig. 3C). Interestingly, one can see that the level of synchrony is systematically higher for the mouse brain, intermediate for the human brain, and lower for the monkey brain. These predictions of the model should be tested by appropriate experiments.

4. Discussion

In this paper, we have shown the integration of AdEx mean-field models into whole-cortex simulations for three species, mouse, monkey and human. For each species, the simulations exhibit the main features of the TVB-AdEx model, as found earlier (Goldman et al., 2020, 2022). In particular, the three models exhibit the same emerging property found in the human brain simulations, namely that when the individual AdEx nodes are set in the asynchronous mode, the ensemble of nodes remains asynchronous. This mode of activity is consistent with the "desynchronized" activity classically found in the awake human brain (Steriade, 2003; Niedermeyer and Lopes da Silva, 2005) and which is also seen in the human and monkey brain in microelectrode recordings which also display asynchronous-irregular states (Dehghani et al., 2016). Similarly, when the AdEx nodes are set to the Up/Down state mode, the activity over the whole cortex synchronizes into a slow oscillatory mode. Here also, this slow oscillatory mode corresponds to the Up & Down states seen in single units in microelectrode recordings in human and

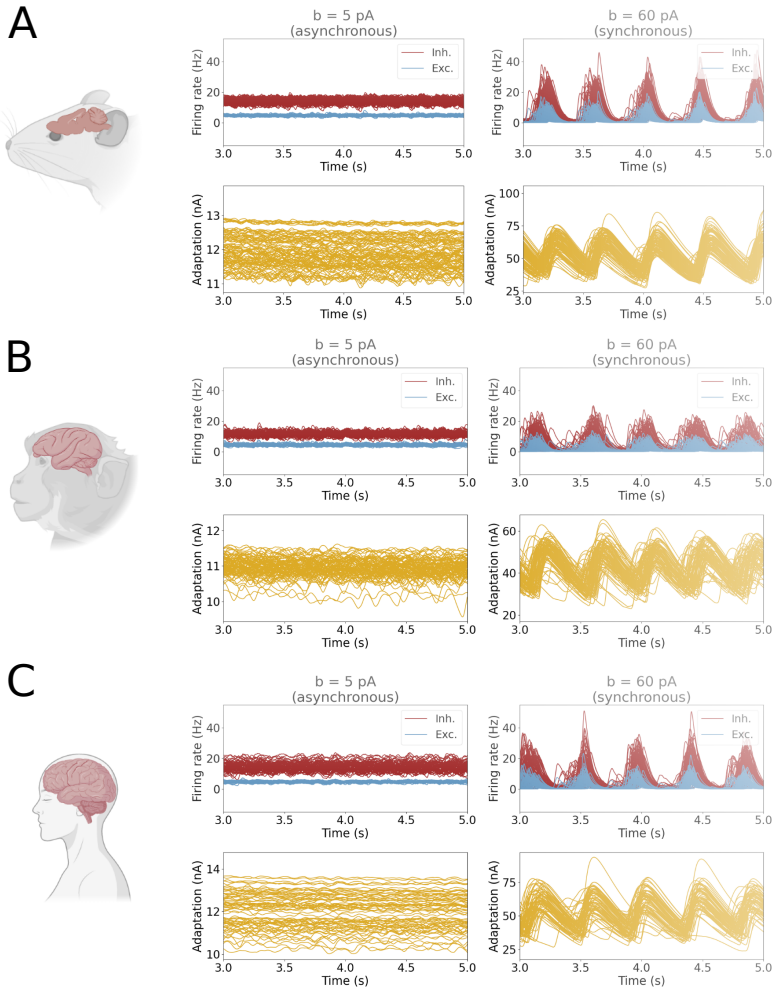

Figure 2: Emergent asynchronous and synchronized slow-wave dynamics in mouse, macaque and human brain models. A: mouse brain, B: macaque brain, C: human brain. In each case, the middle panels show the asynchronous activity resulting from low levels of spike-frequency adaptation (b=5 pA), while the right panels show the slow-wave dynamics obtained for higher levels of spike-frequency adaptation (b=60 pA). The color code is blue for excitatory firing rates, red for inhibitory firing rates, and yellow for mean adaptation. Panel C was modified from Goldman et al. (2022).

monkey during slow-wave sleep (Peyrache et al., 2012; Dehghani et al., 2016). Microelectrode recordings in mice also display the same two states, asynchronous-irregular dynamics during wakefulness and Up & Down state dynamics during slow-wave sleep (Fisher et al., 2016), and similarly in cats (Destexhe et al., 1999).

We believe that the simulations explored here, and for which we provide the python code (Goldman et al., 2023), constitute a very useful tool for the community of computational neuroscientists interested in simulating whole-brain dynamics in mouse, monkey and human. We must note here that the code we provide are codes running within the TVB environment (Jirsa et al., 2017). In addition, we also have implemented versions of these models which can be run online, on the EBRAINS platform. This will allow users to run the models and change the parameters, without even installing TVB, which could be a useful tool as well.

Finally, we would like to mention a few possible extensions to the models explored here. A first extension is to complete the present model, which is only cortical, by other regions, such as thalamus, hippocampus, basal ganglia, cerebellum, etc. Integrating these regions will require the design of mean-field models specific to each brain region, which was done recently for cerebellum (Lorenzi et al., 2022) and is in progress for other brain regions. A second extension is to study other states and other transitions than the ones explored here. For example, there could be oscillatory states (such as beta, or gamma) occurring as responses to sensory stimulation, slow-wave states occurring under anesthesia, or pathological states such as coma or minimal consciousness. To model such states, the procedure is the same as outlined here: start from a spiking network model displaying these new states, then design a mean-field model that can capture this effect, and finally integrate the mean-field at large scales in TVB. We believe that these are interesting directions to explore and that the models proposed here will provide useful tools for this exploration.

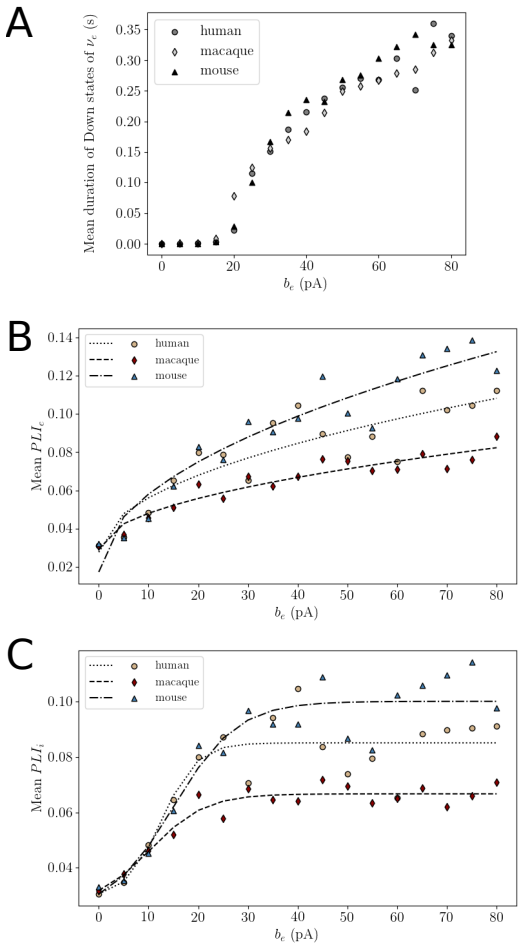

Figure 3: Comparison of the asynchronous and synchronized slow-wave dynamics in mouse, macaque and human brain models. A: Transition between asynchronous and slow-wave dynamics measured by the mean duration of down states. B. Mean phase-lag index (PLI) for excitatory neuron activities for the three species. C. Same as B, but the PLI is shown for inhibitory neuron activities.

Acknowledgments

Research supported by the CNRS and the European Union (Human Brain Project H2020-785907, H2020-945539). We thank Bahar Hazal Yalçinkaya, Trang-Anh Nghiem, David Aquilue, Kevin Ancourt and Viktor Jirsa for their help, support and discussion.

References

Bazhenov, M., Timofeev, I., Steriade, M., Sejnowski, T.J., 2002. Model of thalamocortical slow-wave sleep oscillations and transitions to activated states. Journal of neuroscience 22, 8691–8704.

Brette, R., Gerstner, W., 2005. Adaptive exponential integrate-and-fire model as an effective description of neuronal activity. Journal of Neurophysiology 94, 3637–3642.

Brunel, N., 2000. Dynamics of sparsely connected networks of excitatory and inhibitory spiking neurons. Journal of Computational Neuroscience 8, 183–208.

Cakan, C., Dimulescu, C., Khakimova, L., Obst, D., el, A., Obermayer, K., 2022. Spatiotemporal Patterns of Adaptation-Induced Slow Oscillations in a Whole-Brain Model of Slow-Wave Sleep. Front Comput Neurosci 15, 800101.

Capone, C., di Volo, M., Romagnoni, A., Mattia, M., Destexhe, A., 2019. A state-dependent mean-field formalism to model different activity states in conductance based networks of spiking neurons. bioRxiv , 565127.

Chemla, S., Reynaud, A., di Volo, M., Zerlaut, Y., Perrinet, L., Destexhe, A., Chavane, F., 2019. Suppressive traveling waves shape representations of illusory motion in primary visual cortex of awake primate. Journal of Neuroscience 39, 4282–4298.

Compte, A., Sanchez-Vives, M.V., McCormick, D.A., Wang, X.J., 2003. Cellular and network mechanisms of slow oscillatory activity (< 1 hz) in a cortical network model. Journal of neurophysiology 89, 2707–2725.

Dehghani, N., Peyrache, A., Telenczuk, B., Le Van Quyen, M., Halgren, E., Cash, S.S., Hatsopoulos, N.G., Destexhe, A., 2016. Dynamic balance of excitation and inhibition in human and monkey neocortex. Scientific Reports 6, 23176.

Destexhe, A., 2009. Self-sustained asynchronous irregular states and up–down states in thalamic, cortical and thalamocortical networks of nonlinear integrate-and-fire neurons. Journal of Computational Neuroscience 27, 493.

Destexhe, A., Contreras, D., Steriade, M., 1999. Spatiotemporal analysis of local field potentials and unit discharges in cat cerebral cortex during natural wake and sleep states. Journal of Neuroscience 19, 4595–4608.

El Boustani, S., Destexhe, A., 2009. A master equation formalism for macroscopic modeling of asynchronous irregular activity states. Neural Computation 21, 46–100.

Fisher, S.P., Cui, N., McKillop, L.E., Gemignani, J., Bannerman, D.M., Oliver, P.L., Peirson, S.N., Vyazovskiy, V.V., 2016. Stereotypic wheel

running decreases cortical activity in mice. Nat Commun 7, 13138.

Goldman, J., Sacha, M., Destexhe, A., 2023. Source code for simulating connectome-based models of mouse, monkey and human cerebral cortex. Zenodo ..., ...

Goldman, J.S., Kusch, L., Llorens, D.A., Yalçinkaya, B.H., Depannemaecker, D., Ancourt, K., Nghiem, T.A.E., Jirsa, V., Destexhe, A., 2022. A comprehensive neural simulation of slow-wave sleep and highly responsive wakefulness dynamics. Frontiers in Computational Neuroscience URL: https://doi.org/10.3389/fncom.2022.1058957, doi:10.3389/fncom.2022.1058957.

Goldman, J.S., Kusch, L., Yalçinkaya, B.H., Depannemaecker, D., Nghiem, T.A.E., Jirsa, V., Destexhe, A., 2020. Brain-scale emergence of slow-wave synchrony and highly responsive asynchronous states based on biologically realistic population models simulated in the virtual brain. bioRxiv URL: https://doi.org/10.1101/2020.12.28.424574, doi:10.1101/2020.12.28.424574.

Jirsa, V.K., Proix, T., Perdikis, D., Woodman, M.M., Wang, H., Gonzalez-Martinez, J., Bernard, C., Bénar, C., Guye, M., Chauvel, P., et al., 2017. The virtual epileptic patient: individualized whole-brain models of epilepsy spread. Neuroimage 145, 377–388.

Kötter, R., 2004. Online retrieval, processing, and visualization of primate connectivity data from the cocomac database. Neuroinformatics 2, 127144.

Lorenzi, R.M., Geminiani, A., Zerlaut, Y., Destexhe, A., Gandini Wheeler-Kingshott, C.A., Palesi, F., Casellato, C., D'Angelo, E., 2022. A multilayer mean-field model for the cerebellar cortex: design, validation, and prediction. bioRxiv URL: https://www.biorxiv.org/content/early/2022/11/25/2022.11.24.517708, doi:10.1101/2022.11.24.517708.

Melozzi, F., Woodman, M.M., Jirsa, V.K., Bernard, C., 2017. The virtual mouse brain: A computational neuroinformatics platform to study whole mouse brain dynamics. eNeuro 4, 0111.

Niedermeyer, E., Lopes da Silva, F.H., 2005. Electroencephalography: basic principles, clinical applications, and related fields. Lippincott Williams & Wilkins.

Oh, S.W., Harris, J.A., Ng, L., Winslow, B., Cain, N., Mihalas, S., Wang, Q., Lau, C., Kuan, L., Henry, A.M., et al., 2014. A mesoscale connectome of the mouse brain. Nature 508, 207–214.

Peyrache, A., Dehghani, N., Eskandar, E.N., Madsen, J.R., Anderson, W.S., Donoghue, J.a., Hochberg, L.R., Halgren, E., Cash, S.S., Destexhe, A., 2012. Spatiotemporal dynamics of neocortical excitation and inhibition during human sleep. Proceedings of the National Academy of Sciences of the United States of America 109, 1731–6. URL: http://www.pubmedcentral.nih.gov/articlerender.fcgi?artid=3277175{&}tool=pmcentrez{&}rendertype=abstract, doi:10.1073/pnas.1109895109.

Ritter, P., Schirner, M., McIntosh, A.R., Jirsa, V.K., 2013. The virtual brain integrates computational modelling and multimodal neuroimaging. Brain Connect. 3, 121–145.

Sanchez-Vives, M.V., McCormick, D.A., 2000. Cellular and network mechanisms of rhythmic recurrent activity in neocortex. Nature neuroscience 3, 1027.

Shen, K., Bezgin, G., Schirner, M., Ritter, P., Everling, S., McIntosh, A.R., 2019. A macaque connectome for large-scale network simulations in thevirtualbrain. Scientific Data 6. doi:10.1038/s41597-019-0129-z.

Silva Pereira, S., Hindriks, R., Mühlberg, S., Maris, E., van Ede, F., Griffa, A., Hagmann, P., Deco, G., 2017. Effect of field spread on resting-state magneto encephalography functional network analysis: A computational modeling study. Brain Connectivity 7, 541–557.

Steriade, M., 2003. Neuronal substrates of sleep and epilepsy. Cambridge University Press.

Van Essen, D.C., Ugurbil, K., Auerbach, E., Barch, D., Behrens, T.E., Bucholz, R., Chang, A., Chen, L., Corbetta, M., Curtiss, S.W., et al., 2012. The human connectome project: a data acquisition perspective. Neuroimage 62, 2222–2231.

Van Vreeswijk, C., Sompolinsky, H., 1996. Chaos in neuronal networks with balanced excitatory and inhibitory activity. Science 274, 1724–1726.

di Volo, M., Romagnoni, A., Capone, C., Destexhe, A., 2019. Biologically realistic mean-field models of conductance-based networks of spiking neurons with adaptation. Neural Computation 31, 653–680.

Wilson, H.R., Cowan, J.D., 1972. Excitatory and inhibitory interactions in localized populations of model neurons. Biophysical Journal 12, 1–24.

Zerlaut, Y., Chemla, S., Chavane, F., Destexhe, A., 2018. Modeling mesoscopic cortical dynamics using a mean-field model of conductance-based networks of adaptive exponential integrate-and-fire neurons. Journal of Computational Neuroscience 44, 45–61.